Earth and Planetary Science Letters 442 (2016) 108–120

Contents lists available at ScienceDirect

Earth and Planetary Science Letters

www.elsevier.com/locate/epsl

Frontiers paper

Thermal effects of impact bombardments on Noachian Mars

Oleg Abramov [a], Stephen J. Mojzsis [b,c,*]

[a] United States Geological Survey, Astrogeology Science Center, 2255 N. Gemini Dr., Flagstaff, AZ 86001, USA
[b] Collaborative for Research in Origins (CRiO), Department of Geological Sciences, University of Colorado, UCB 399, 2200 Colorado Avenue, Boulder, CO 80309-0399, USA
[c] Institute for Geological and Geochemical Research, Research Center for Astronomy and Earth Sciences, Hungarian Academy of Sciences, 45 Budaörsi Street, H-1112 Budapest, Hungary

ARTICLE INFO

Article history:
Received 10 August 2015
Received in revised form 24 January 2016
Accepted 17 February 2016
Available online 15 March 2016
Editor: M.M. Hirschmann

Keywords:
Mars
bombardment
crust
impacts
thermal modeling
habitability

ABSTRACT

Noachian (prior to ca. 3700 Ma) terranes are the oldest and most heavily cratered landscapes on Mars, with crater densities comparable to the ancient highlands of the Moon and Mercury. Intense early cratering affected Mars by melting and fracturing its crust, draping large areas in impact ejecta, generating regional-scale hydrothermal systems, and increasing atmospheric pressure (and thereby, temperature) to periodically re-start an otherwise moribund hydrological cycle. Post primary-accretionary bombardment scenarios that shaped early Mars can be imagined in two ways: either as a simple exponential decay with an approximately 100 Myr half-life, or as a "sawtooth" timeline characterized by both faster-than-exponential decay from primary accretion and relatively lower total delivered mass. Indications are that a late bombardment spike was superposed on an otherwise broadly monotonic decline subsequent to primary accretion, of which two types are investigated: a classical "Late Heavy Bombardment" (LHB) peak of impactors centered at ca. 3900 Ma that lasted 100 Myr, and a protracted bombardment typified by a sudden increase in impactor flux at ca. 4100–4200 Ma with a correspondingly longer decay time ($\leq$400 Myr). Numerical models for each of the four bombardment scenarios cited above show that the martian crust mostly escaped exogenic melting from bombardment. We find that depending on the chosen scenario, other physical effects of impacts were more important than melt generation. Model output shows that between 10 and 100% of the Noachian surface was covered by impact craters and blanketed in resultant (hot) ejecta. If early Mars was generally arid and cold, impact-induced heating punctuated this surface state by intermittently destabilizing the near-subsurface cryosphere to generate regional-scale hydrothermal systems. Rather than being deleterious to the proclivity of Noachian Mars to host an emergent biosphere, this intense early impact environment instead enhanced the volume and duration of its surface/subsurface geophysical habitable zone.

1. Introduction

It is widely recognized that in the solar system's first billion years, impact processes greatly affected the surfaces of the solid planetary bodies, be they composed of ices or silicates (Melosh, 1989). As such, investigations formulated to explore the effects of early bombardment to Earth's initial thermal, mechanical, chemical and biological state have long been a fertile area of study (e.g. Öpik, 1960; Hartmann, 1966; Sleep and Zahnle, 1998). Profound chemical and mechanical modifications of its ancient crust are expected to have occurred due to impacts. All the more so for a small (0.107 $M_{\oplus}$), old (Dauphas and Pourmand, 2011) and cold (e.g. Carr and Head, 2010) world like Mars that has always been situated at the outer edge of our solar system's habitable zone (Hart, 1979), the early bombardment regime imposed strong controls on planet-wide geophysical states. Compared to Mars, Earth's crust is very young and consequently records practically nothing of the bombardment epoch (e.g. Trail et al., 2007); the average age of terrestrial oceanic crust is only about 70 Ma, whereas that of the continents is close to 2500 Ma (e.g. Taylor and McLennan, 1995). On Mars, however, about 60% of the crust dates from before about 3700 Ma (e.g. Neumann et al., 2004). At an average crustal depth of about 60 km (Wieczorek and Zuber, 2004), this corresponds to a theoretical Pre-Noachian/Noachian crustal volume of approximately 5×10^9 km^3. On Earth, the equivalent late Hadean–Eoarchean (4000–3650 Ma) crustal inventory is a mere 1×10^{-5}

* Corresponding author at: University of Colorado, Department of Geological Sciences, 2200 Colorado Ave., Boulder, CO 80309-0299, USA. Tel.: +1 303 492 5014; fax: +1 303 492 2606.
E-mail address: mojzsis@colorado.edu (S.J. Mojzsis).

http://dx.doi.org/10.1016/j.epsl.2016.02.035
0012-821X/

of the total volume of continental crust (Nutman et al., 2001), which leads to a rough estimate of $\sim 1.5 \times 10^4$ km^3. Evidently, Mars preserves hundreds of thousands of times ($\sim$340,000$\times$) more "Hadean" crust than does Earth. Aside from the lifeless Moon, Mars is the most accessible repository in our solar system of processes to have operated on the inner (terrestrial-type) planets in the first half-billion years. It shows abundant evidence for how intense modifications from bombardment strictly controlled a rocky world's capacity to host environments suitable for the emergence and sustainability of a biosphere. Its richness and variety of fluvial features (e.g. Carr, 1999) as well as evidence for long episodes of aqueous alteration (e.g. Ehlmann et al., 2009) demonstrates conclusively that Noachian Mars was episodically wet before about 3700 Ma (Carr, 2012). In this context, the combination of water and impact-delivered heat (and to a lesser degree, volcanism) should have driven long-lived extensive and ubiquitous hydrothermal systems on early Mars (e.g. Abramov and Kring, 2005).

Impact-induced effects on Mars included: (i) structural modifications to the lithosphere including some that involved an entire hemisphere (e.g. Andrews-Hanna et al., 2008; cf. Melosh, 2008); (ii) melt production at the regional (10 s to 100 s of km) to global scale (1000 s of km); (iii) melt mixing and differentiation of impact melt sheets; (iv) implantation of shock-deposited heat that lingered on in the lithosphere and mantle for millions of years (Abramov and Mojzsis, 2009); (v) generation of thick and overlapping regional and global layers of hot ejecta (e.g. Sleep and Zahnle, 1998); (vi) compositional changes and resultant modifications to the surface zone via delivery of cometary and asteroidal materials (e.g. Flynn, 1996) that probably included the supply of prebiotically important molecules (e.g. Wright et al., 1989); and (vii) changes to primordial atmospheric compositions and densities, and thereby of paleoclimate (e.g. Toon et al., 1982), which involved the catastrophic release of water vapor into the atmosphere from heating of Mars' surface/sub-surface cryosphere (e.g. Segura et al., 2002).

The earliest styles of bombardment to have affected Mars immediately following its formation are modeled in this work as either a:

(i) *Classical* post-accretionary bombardment characterized by an exponential decay of the impactor flux with a 100 Myr half-life (Ivanov et al., 2002)
(ii) *"Sawtooth"* post-accretionary bombardment with a faster-than-exponential decay from primary accretion compared to the *Classical* modality, and relatively lower total accreted mass. This model was introduced by Morbidelli et al. (2012; cf. Turner, 1979) and developed further by Marchi et al. (2014).

We also focus on two later enhancements to the bombardment flux superimposed on a long post-accretionary decline:

(i) *Classical* "late heavy bombardment" spike in impactors, centered at 3900 Ma with a duration of approximately 100 Myr (Turner et al., 1973; Tera et al., 1974; Wetherill, 1975; Ryder, 1990, 2002).

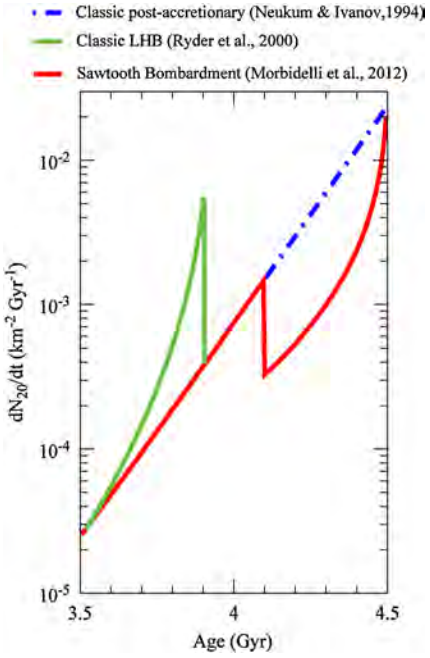

Fig. 1. Timeline of martian bombardment scenarios modeled in this work. The Sawtooth bombardment timeline includes both Sawtooth post-accretionary (sPA, pre-4.1 Ga) and Sawtooth LHB (sLHB, 4100 Ma and later) scenarios. This figure has been modified from Morbidelli et al. (2012) for fluxes to Mars.

(ii) *Sawtooth*-like late heavy bombardment scenario distinguished by a sharp rise in the number of impacts at ca. 4100–4250 Ma (e.g. Hopkins and Mojzsis, 2015) with overall relatively lower delivered mass than the *Classical* model, followed by a shallow ramp in the flux with correspondingly longer duration of bombardment ($\sim$400 Myr). Afterwards, there is a long tail of decay of the impactor population (e.g. Bottke et al., 2010) that extended well into Earth's Proterozoic eon (corresponding to Mars' middle Amazonian period; Tanaka, 1986).

A timeline illustrating the relationships between the bombardments outlined above is presented in Fig. 1.

Next, we review the four different bombardment scenarios outlined above: two early bombardments and two late bombardments, by comprehensively assessing the thermal effects of each to the martian crust (Table 1). The output of our global bombardment models is thereafter used to evaluate the thermal state of Mars' crust in the Noachian and to gauge its past ability to have accommodated an alien biome.

1.1. Modeled bombardments

1.1.1. Classical post-accretionary (cPA)

After the major planet-building phase of accretion ceased, numerous leftover planetesimals populated the solar system and

Table 1
Summary of statistics for the four bombardment scenarios on early Mars. Total melting in the upper 20 km of the crust during the bombardment is shown, and is calculated using the high-resolution static model. Mean values between the 1 °C and −63 °C surface temperatures are shown. Resurfacing is calculated based on the area of the final crater.

Bombardment type		Start time (Ga)	End time (Ga)	Total mass delivered (kg)	Largest impactor (km)	Percent of crust melted	Percent resurfaced
Post-accretionary	Classical (cPA)	4.5	4.1	6.5×10^{20}	492	3.9%	100%
	Sawtooth (sPA)	4.5	4.1	1.6×10^{20}	310	1.1%	46%
Late heavy bombardment	Classical (cLHB)	3.9	3.8	1.0×10^{20}	246	0.8%	36%
	Sawtooth (sLHB)	4.1	3.7	2.8×10^{19}	196	0.2%	10%

were depleted from initially high impact fluxes (e.g., Hartmann, 1966). Earlier estimates of the impact rate as a function of time for the inner solar system were based on observations of lunar craters and extrapolated to other planets. The lunar production rate used herein and applied to Mars was originally proposed by Neukum (1983), and later discussed in more detail by Neukum and Ivanov (1994), and Neukum et al. (2001). The relation that describes this post-accretionary exponential decay was recently revisited and revised by Morbidelli et al. (2012), and extrapolated before ca. 4100 Ma to the approximate time of the Moon's formation at about 4500 Ma to be:

$$dN_{20}/dt = 2.7 \times 10^{-16} e^{6.93t} + 5.9 \times 10^{-7} \quad (1)$$

where N_{20} refers the number of craters larger than 20 km in diameter per km^2, and t is time in Giga-years. Although this expression is unconstrained by observational data past 4100 Ma (see Werner, 2014), it is used in this review paper as an example of a classic crater chronology-based model. The consequences of this approach are compared and contrasted to the more recent *Sawtooth* model described below.

1.1.2. Sawtooth post-accretionary (sPA)

Along with the cPA bombardment scenario described above, we model a *Sawtooth* post-accretionary bombardment characterized by faster-than-exponential decay and reduced total mass compared to the *Classical* (cPA) model. The sPA scenario attempts to correct perceived deficiencies in the simple exponential decay model, specifically the difficulties of reproducing it with dynamic models using known projectile populations, and the discrepancy between the models' predicted impact fluxes and the observed concentrations of highly-siderophile elements (HSEs) in lunar rocks (Walker, 2009). The equation used to describe the sPA bombardment on the Moon is provided by Morbidelli et al. (2012) as:

$$dN_{20}/dt = 2.5 \times 10^{-2} e^{-[(4.5-t)/0.003]^{0.34}} \quad (2)$$

for the bombardment regime between about 4500 Ma and 4100–4200 Ma (Fig. 1).

In our analysis, we adjusted the lunar crater production function for Mars by multiplying by a factor of 2.76, as discussed later (sec. 3.1). Furthermore, in all impact models for Mars, a final crater diameter of 20 km corresponds to a transient crater diameter of ~15 km (Abramov and Kring, 2005) and a projectile diameter of ~1.4 km (Schmidt and Housen, 1987) assuming a silicate impactor striking at 10 km s^{-1} at an angle of 45° (Sec. 3.3).

1.1.3. Classical late heavy bombardment (cLHB)

Two types of LHB to Mars are modeled in this work. The first is a *Classical* (cLHB) baseline scenario that was used by Abramov and Mojzsis (2009) and originally applied to the Hadean transition on Earth. It is represented by a well-defined "spike" in the number of impacts centered at ca. 3900 Ma, with a duration of ~100 Myr at a relatively constant flux.

A large body of previous research has shown that many lunar rocks were altered by shock-metamorphism, or brought to melting, in impact-induced thermal events well after primary accretion ceased; many (but not all, see Hopkins and Mojzsis, 2015) ages group around and/or do not exceed ca. 3850–3900 Ma. This observation holds true for both thermal alteration ages of lunar crust (e.g., Turner et al., 1973; Tera et al., 1974) and impact melts returned by the Apollo and Luna missions, as well as for lunar meteorites. One interpretation of these data is that they record a dramatic increase in the number of impacts in a relatively brief time span of 20 to 200 Myr (e.g., Wetherill, 1975) historically termed *late lunar cataclysm*, and more commonly, *late heavy bombardment* (hereafter, LHB). Estimates for asteroidal and cometary material accreted by the Moon and Earth during the cLHB are ~6×10^{18} and ~10^{20} kg, respectively (e.g., Levison et al., 2001).

Evidence for an LHB beyond the Earth–Moon system continues to increase. Meteorites from multiple bodies in the asteroid belt, in particular those presumed to be from 4Vesta (reviewed in Hopkins and Mojzsis, 2015) as well as the ancient martian meteorite ALH84001, also seem to show effects of impact-induced metamorphism at ~3900 Ma (e.g., Bogard, 1995; Ash et al., 1996; Kring and Cohen, 2002; Swindle et al., 2009; Marchi et al., 2013). Analyses of the oldest terrestrial zircons are also (arguably) suggestive of a direct signal of later impact bombardments, as they record discordant U–Pb ages clustered at ca. 3950 Ma (Trail et al., 2007; Abbott et al., 2012; Bell et al., 2014). What is less clear is whether these ages are part of a spike, or are associated with the last vestiges of a long tail of enhanced bombardments (Hopkins and Mojzsis, 2015).

The contemporary population structure of the main asteroid belt can be explained by late stage giant planet migration (Minton and Malhotra, 2009) as predicted in the "Nice model" (Gomes et al., 2005; Tsiganis et al., 2005). The Nice model and its successors (Morbidelli et al., 2012; Marchi et al., 2012, 2014) provide a physically plausible mechanism for the LHB from the migration of the outer planets and suggest a new LHB timeline discussed below. Significantly, the Nice model for giant planet migration lacks a strict temporal requirement. Be that as it may, the interpretation of a Nice model origin for the LHB is debated (e.g., Kaib and Chambers, 2016) at least partly due to the paucity of data for that time that is strongly dominated by a complex record from the Moon. Hence, understanding of the nature and tempo of the late bombardment to the inner solar system as a whole, and the veracity of the various dynamical models that have been formulated to explain it, would benefit from studies of martian bombardment.

1.1.4. Sawtooth-like late heavy bombardment (sLHB)

The second type of LHB we modeled is a variant typified by a Nice model inspired near-instantaneous increase in the number of impacts at ca. 4100 Ma, overall lower delivered mass, and a longer duration, with exponential decay extending from Earth's Eoarchean era (3850–3600 Ma) well into the post-2500 Ma Proterozoic eon (Morbidelli et al., 2012; Bottke et al., 2012). As illustrated in Fig. 1, the sLHB follows the same exponential decay curve described in Eq. (1) for the *Classical* post-accretionary model (cPA), but for the time after about 4100 Ma. Therefore, combining it with the cPA scenario would result in no obvious LHB-type increase in impact flux. It is noteworthy that, while Morbidelli et al. (2012) reported that the Nice/E-belt model predicts that the age of Nectaris is 4100–4200 Ma, they chose 4100 Ma as the start of the Sawtooth timeline for lunar bombardment, based on earlier radiogenic estimates of the age of Nectaris basin (e.g. Schaeffer and Husain, 1974; Maurer et al., 1978). We note that these earlier age estimates are from mixed radiogenic systems, and are therefore open to substantial revision (e.g. Hopkins and Mojzsis, 2015). For coherence with the Morbidelli et al. (2012) and Marchi et al. (2014) chronologies, we use ca. 4100 Ma timeline in our sLHB model.

2. Model description

2.1. Three-dimensional transient heating

The global cratering model originally formulated by Abramov and Mojzsis (2009) and updated in Abramov et al. (2013) for the Hadean Earth, was modified and applied it to the four bombardment-era scenarios for Noachian Mars described above. The inputs for the three-dimensional transient heating model, including the location, diameter, and velocity of each impact, are

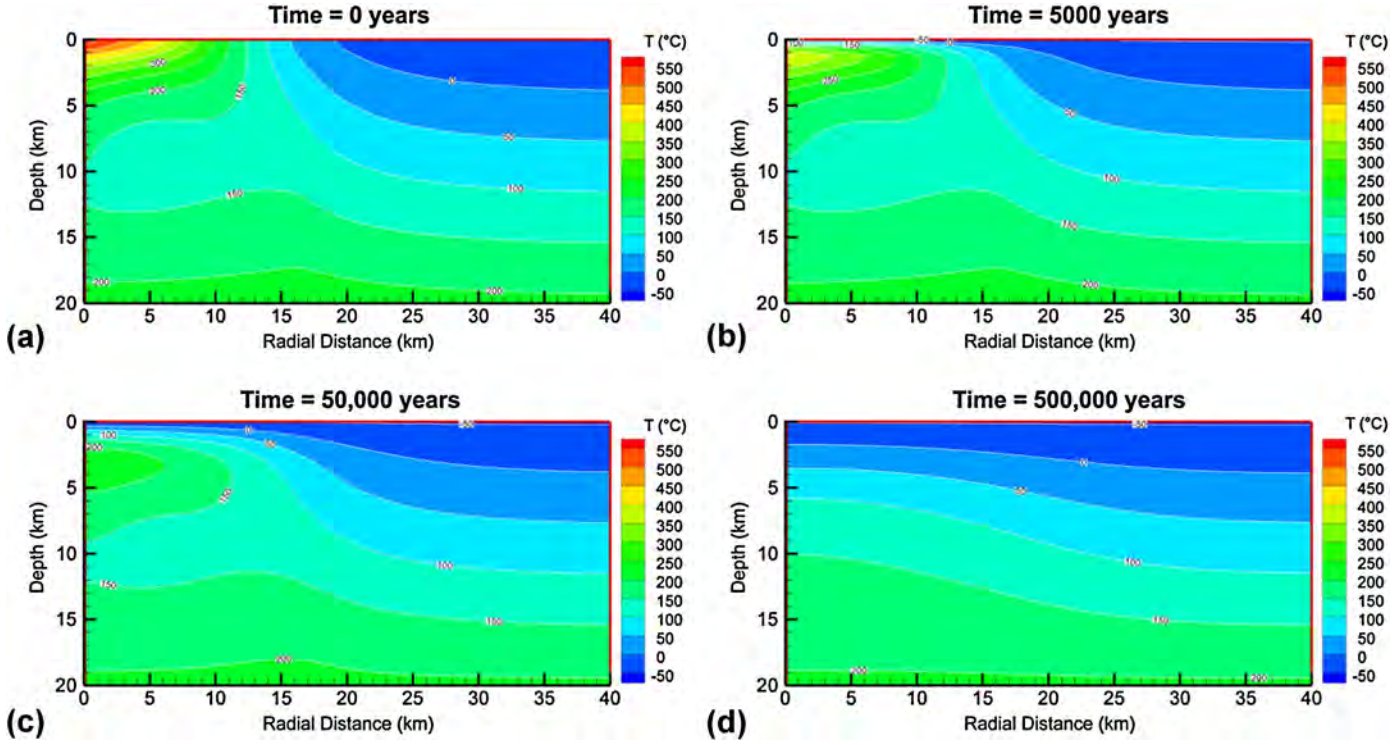

Fig. 2. Conductive and radiative cooling of a 60-km crater on Mars. Note the rapid cooling of the near-surface. This calculation is carried out for thousands of craters in the three-dimensional models. (For interpretation of the colors in this figure, the reader is referred to the web version of this article.)

generated by stochastic cratering (Richardson et al., 2005). This stochastic cratering model populates all or part of the martian surface with craters as a function of time within a field of constraints established from both models and observations (Sec. 3). For each crater in the model, a temperature field is calculated using analytical expressions for shock deposited heat and central uplift, as described in detail in Abramov et al. (2013). After the crater's thermal field is entered into a three-dimensional model representing the martian lithosphere, it is allowed to cool by conduction in the subsurface and radiation/convection at the atmosphere interface (Fig. 2). The geometrical approximation of the whole lithosphere as a cuboid is valid because the lithosphere is a small fraction of the overall planetary diameter, and thus, its volume does not decrease significantly with depth. The model neglects any latitude-dependency of the impacts. In the code, crustal volumes within the temperature ranges of interest are monitored in time-steps, and the output tabulated (see: Supplementary online material).

2.2. Two-dimensional static heating model

In this technique, the temperature distribution library is used to calculate the volume of crust that is heated above a specified temperature for every crater predicted by the stochastic cratering model. Additional inputs used in this analysis are surface temperature, geothermal gradient and crustal thickness. This simple model assumes that impacts do not overlap and neglects any post-impact conductive heat transfer in the subsurface, which results in significant savings in computational time. The tradeoff to this approach is a higher overall resolution, which allows the inclusion of impactors as small as 1 km in diameter, as opposed to 2.5 km in diameter for the three-dimensional transient heating model.

2.3. Comparison to hydrocode models

Hydrocodes provide cratering simulations that faithfully reproduce shock pressure fields observed in nature (e.g., Pierazzo and Collins, 2004). These simulations are extremely computationally

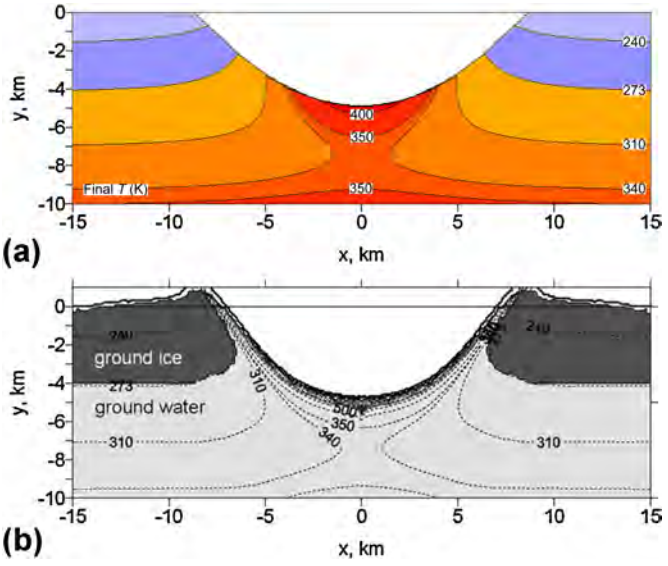

Fig. 3. (a) Transient crater and temperature distribution generated by the analytical methods described in this paper for a vertical impact of a 2 km asteroid at 8 km/s on Mars. Final crater would be ~30 km in diameter. (b) For comparison, transient crater and temperature distribution generated by Pierazzo et al. (2005) using hydrocodes SOVA (for early stages) and SALEB (for late stages). The initial conditions are identical. (For interpretation of the colors in this figure, the reader is referred to the web version of this article.)

intensive, however, and are thus prohibitive for the purposes of modeling tens of thousands to millions of events at the scale of an entire planet (e.g., Marchi et al., 2014). As a simple sensitivity test between the two techniques, we performed an experiment (Fig. 3) to compare a sample temperature distribution for a ~30-km diameter transient crater on Mars. The result illustrates well the agreement between the analytical method of Kieffer and Simonds (1980), implemented by Abramov and Mojzsis (2009) and Abramov et al. (2013), with the hydrocode model of Pierazzo et al. (2005).

Although the analytical method utilizing the Murnaghan equation of state (Kieffer and Simonds, 1980) employed here only accounts for shock-deposited heat and neglects frictional heating, the overall agreement between the two methods is within ∼10%. We interpret this to mean that the frictional heating component of the cratering process is relatively minor and can be neglected for our purposes of assessing the regional- to global-scale impact environment. Additional caveats of analytical approximations to hydrocode modeling, such as decompression melting, are discussed in Marchi et al. (2014) and references therein.

3. Input parameters

3.1. Delivered mass

There are numerous lines of evidence that impact flux, expressed as impacts per unit area per unit time, is higher on Mars than on the Earth (e.g., JeongAhn and Malhotra, 2015). Simulations of a stirred asteroid belt show that the LHB impact flux was higher on Mars than the Earth by a factor of ∼4.5 (Horner et al., 2009). Based on the number of observed impacts on Mars, an impact flux factor of ∼4.5 could be interpreted to mean that all observed martian impact basins, including some controversial quasi-circular depressions (e.g., Frey, 2008) are all a consequence of the LHB (De Niem et al., 2012). We deem this unlikely owing to the fact that our current understanding of the record of early impact bombardments precludes the possibility that Mars incurred *no* large impacts outside of LHB time. Instead, we use a more conservative Mars/Earth impact flux ratio of 1.75, and Mars/Moon impact flux ratio at 2.76, as advocated by Le Feuvre and Wieczorek (2011). This alternative flux ratio represents a long-term average, and is thus broadly applicable to post-accretionary bombardment. When adjusted for planetary surface areas, this equates to 21 impacts on the Earth and 10.5 impacts on Mars for every impact on the Moon.

From this foundation, we now estimate total delivered mass to Mars in the four bombardment scenarios in Table 1. For the classical post-accretionary (cPA), Sawtooth post-accretionary (sPA), and Sawtooth-like LHB (sLHB) scenarios, we multiply Eq. (1) and Eq. (2) by a factor of 2.76. The modified production function is then coupled with the size-frequency distribution described below (Sec. 3.3) to estimate total delivered masses. Abramov and Mojzsis (2009) and Abramov et al. (2013) previously explored the classical LHB (cLHB) scenario and estimated the total mass delivered to the Hadean Earth at 2×10^{20} kg (e.g. Levison et al., 2001). When multiplied by the Mars/Earth impact flux ratio of 1.75 and 0.28 Mars/Earth surface area ratio, this value corresponds to a total delivered cLHB mass of 1×10^{20} kg to Noachian Mars. These values should be regarded as loosely constrained estimates.

3.2. Bombardment timing and duration

As shown in Table 1, the classical LHB (cLHB) scenario assumes the extent of the LHB is ∼100 Myr, with a constant bombardment flux between 3900–3800 Ma. The duration for the Sawtooth LHB scenario is 400 Myr, with the flux declining between 4100–3700 Ma as described by Eq. (1) (Morbidelli et al., 2012). Both the classical and Sawtooth post-accretionary bombardments are ∼400 Myr in duration from ca. 4500 Ma to ca. 4100 Ma, with fluxes declining as described by Eq. (1) and Eq. (2), respectively (Morbidelli et al., 2012).

3.3. Impactor parameters

There are some indications that both post-accretionary and LHB impactors were dominated by a population with a size/frequency distribution similar to that of the present-day main belt asteroids (Strom et al., 2005). Further research suggests that present-day size/frequency distribution (SFD) is unlikely to have changed significantly since the LHB (Bottke et al., 2005). We therefore employ the main belt SFD in this work, and assume bombardments by rocky asteroids with a mean density of 3000 $\mathrm{kg\,m^{-3}}$. A typical Mars asteroid impact velocity of 10 $\mathrm{km\,s^{-1}}$ (Ivanov, 2001) and the most probable impact angle of 45° (e.g., Shoemaker, 1962) are used in all simulations. In both cases, representative values are used because the intent of this work is to provide an average profile of how impacts affect Mars.

Table 2
Summary of target properties. A basaltic lithology is assumed. Thermal conductivity is given in the HEATING materials library (Childs, 1993); references and/or justifications for other values are given in the text.

Parameter	Value(s)	Units
Pressure derivative of the bulk modulus	5.5	Unitless
Adiabatic bulk modulus at zero pressure	19.3×10^9	Pa
Heat capacity	800	$\mathrm{J\,kg^{-1}\,°C^{-1}}$
Density	3000	$\mathrm{kg\,m^{-3}}$
Latent heat of fusion	400	$\mathrm{kJ\,kg^{-1}}$
Liquidus temperature	1250	°C
Solidus temperature	1100	°C
Surface temperature	−63.1	°C
Geothermal gradient	13	$\mathrm{°C\,km^{-1}}$
Thermal conductivity	2.5	$\mathrm{W\,m^{-1}\,°C^{-1}}$

3.4. Crustal target parameters

Rock density, thermal conductivity, and heat capacity are assumed to be those of basalt, the dominant lithology of the martian crust (e.g., McSween et al., 2003). Pressure derivative of the bulk modulus is 5.5, and adiabatic bulk modulus at zero pressure is 19.3×10^9 Pa (Gault and Heitowit, 1963). All target properties are summarized in Table 2. The recent discovery of granitoids on Mars by Sautter et al. (2015) opens the possibility that some unknown portion of the oldest martian crust also contains felsic lithologies of broadly granitic character.

3.5. Surface temperature and geothermal gradient

There is disagreement over the nature of the climate of Noachian Mars, specifically whether it was generally cold with perhaps short episodes of warming (e.g., Fairén, 2010) or warm (e.g., Craddock and Howard, 2002); we test both scenarios. For the "warm early Mars" scenario, we assume a surface temperature of 1 °C, whereas for the "cold early Mars" scenario, we take a surface temperature of −63 °C. Geothermal gradient is set to $13\,\mathrm{°C\,km^{-1}}$ (Babeyko and Zharkov, 2000). The results of our output are generally insensitive to small (±10%) changes in these physical parameters.

4. Results

Mars' smaller surface area ($A_{\oplus} = 0.28$) was impacted by approximately half the mass Earth received, and experienced a cratering density about twice that of terrestrial Hadean values during both post-accretionary and LHB bombardments. Most of Mars' surface area becomes resurfaced in our baseline LHB (cLHB) scenario, and all of it in the baseline post-accretionary bombardment (cPA) with cratering at saturation. The average impact velocity on Mars is about half that of Earth, and thus, average energy delivered per unit area is less by a factor of four. As was concluded for model runs of Hadean Earth (Abramov and Mojzsis, 2009), most of the crust of Noachian Mars escaped *melting* by either a post-accretionary bombardment or the LHB even if it was *mechanically* destroyed. Based on the constraints of mass and size-frequency distribution, the largest impacting object in our baseline

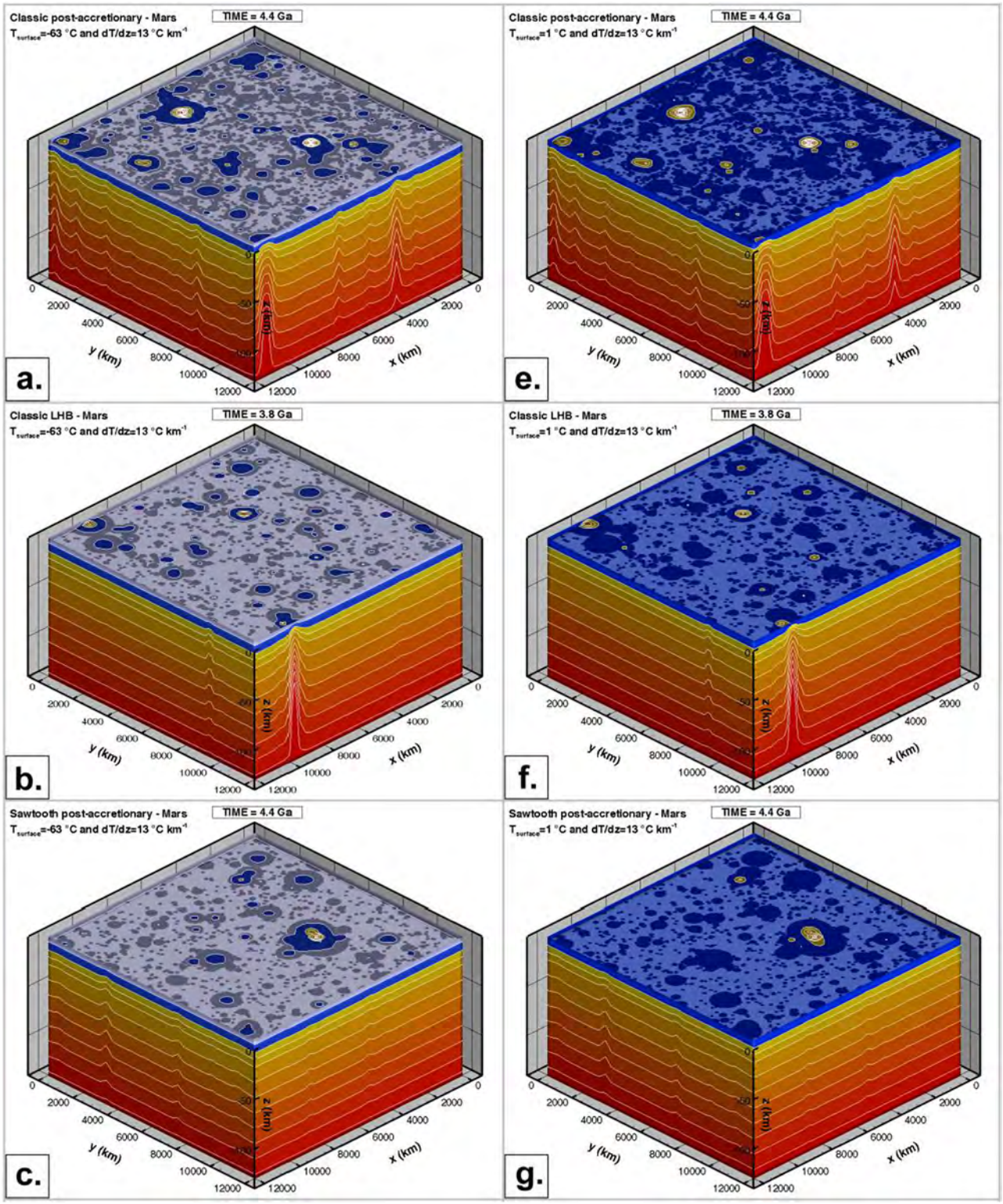

Fig. 4. (*Continued on the next page*) A three-dimensional thermal model representing the upper 140 km of Mars 100 Myr into the bombardment. Only impactors larger than 2.5 km in diameter are included. Dark circles indicate crater locations, light blue areas indicate the extent of the cryosphere, and dark blue areas indicate the extent of the subsurface habitable zone. The upper boundary shows temperatures at a depth of 4 km. (a–d) Classical post-accretionary (cPA), classical LHB (cLHB), Sawtooth post-accretionary (sPA), and Sawtooth LHB scenarios (sLHB), respectively, with a surface temperature of $-63\,^{\circ}\mathrm{C\,km^{-1}}$. (e–h) Classical post-accretionary (cPA), classical LHB (cLHB), Sawtooth post-accretionary (sPA), and Sawtooth LHB scenarios (sLHB), respectively, with a surface temperature of $1\,^{\circ}\mathrm{C\,km^{-1}}$. (For interpretation of the references to color in this figure legend, the reader is referred to the web version of this article.)

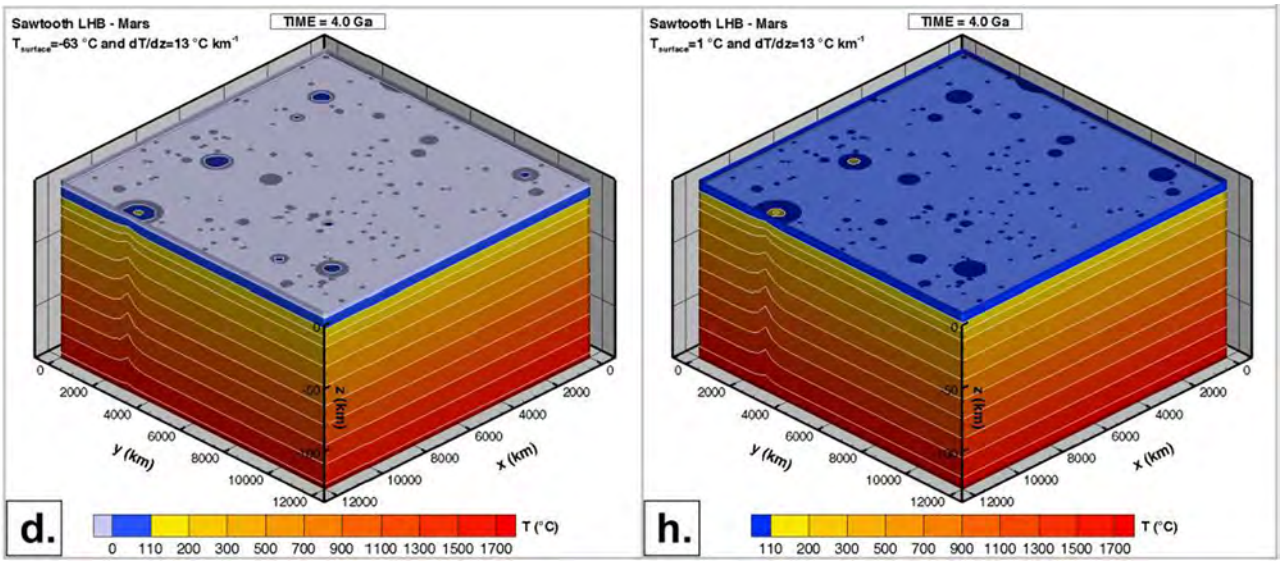

Fig. 4. (*continued*)

LHB model (cLHB) is ∼250 km in diameter, which generates a crater ∼1800 km across (approximately the size of Argyre Basin; cf. Dohm et al., 2015). The largest impactor in our baseline post-accretionary (cPA) model is ∼490 km in diameter. The resulting crater from such an object would have exceeded Hellas Basin in size (diameter, 2300 km).

A graphical overview of the results from models representing the four bombardment scenarios and two surface temperature conditions are presented in Fig. 4 at 100 Myr into the bombardment, and Fig. 5 at the end of the bombardment simulation. These results are from the three-dimensional transient heating model (Sec. 2.1). Note the deflection of the isotherms at the lateral boundaries of the model due to impacts, and that, although a relatively large number of craters have formed, most have quickly cooled to below 100 °C at the model's upper boundary layer set to a depth of 4 km. The classical post-accretionary (cPA) scenario has the largest amount of mass delivered, and a larger number of total impacts and hot craters is present. A substantial fraction of the near-subsurface is heated above 100 °C in the early stages of the cPA bombardment, and at the end of the simulation, impact craters essentially saturate the surface. Notwithstanding these surface modifications, our model also shows that less than one percent of the upper ∼20 km of the crust is brought to melting 100 Myr into the bombardment. In the classical LHB (cLHB) scenario, significantly fewer craters are present, as the delivered mass is 6–7 times less than in cPA (Table 1). The results at 100 Myr and the end of the bombardment are identical, as the entire cLHB event takes 100 Myr. The outcomes at 100 Myr for the Sawtooth post-accretionary bombardment (sPA) scenario strongly resemble the classical LHB (cLHB) bombardment, due to a similar delivered mass. At the end of the ∼400 Myr-long Sawtooth post-accretionary bombardment, however, essentially no warm craters remain. This is due to relatively long intervals between impacts and comparatively short cooling times within the declining impact flux. The Sawtooth LHB (sLHB) scenario is characterized by the lowest delivered mass, fewest formed craters, with only one crater harboring a potential hydrothermal system containing liquid water to a depth of 4 km. Comparisons of our models that use a −63 °C surface temperature to those set at 1 °C reveal that the latter have significantly fewer impact-induced hotspots that stand out from the warmer background temperatures.

Impact melt volumes within the upper 20 km of the crust were computed and tabulated throughout the course of the simulations (Fig. 6; Supplementary online material). Abrupt peaks and the long dwell time between them indicate that most melting is caused by a few large impacts above what must have been a frequent rain of smaller bolides. Following a basin-forming impact, the amount of melt present decreases substantially due to extended cooling times before another basin is formed. In the cPA scenario, which has the highest delivered mass, a maximum of ∼0.5% of the upper crust is molten at any given time. We find that if there is marginally more melt generated in the warm early Mars model with a surface temperature of 1 °C.

The melting results described above were derived from the transient heating model, which included exclusively impactors larger than 2.5 km. In order to further test these results and assess the relative importance of smaller impactors, a high-resolution static model (Section 2.2) was used to calculate cumulative crustal heating. The results, presented in Table 1, are in excellent agreement with those shown in Fig. 6. This validates the model and also points to the relative inefficacy of small impactors to global heating.

We now evaluate the geophysical habitable volumes (Abramov and Mojzsis, 2009) within the upper 4 km of the martian crust as the various bombardments progressed. To do so, we invoke a hypothetical biome composed of meso-, thermo- and hyperthermophilic microorganisms. For the cold Noachian Mars scenario (Fig. 7) the general trend is for all geophysical habitable volumes to increase in the early stages of the bombardment as the impacts melt the icy cryosphere, and to then decline with decreasing impact fluxes. The exception is the cLHB, which is modeled with a constant flux and therefore shows no decline as the bombardment commences. Geophysical habitable volumes of Mars' early crust reached maxima of $\sim 1.2 \times 10^7$ km^3 and $\sim 4 \times 10^6$ km^3 for cPA bombardment and cLHB, respectively. For comparison, the total volume of the upper 4 km of Mars' crust is 7.6×10^8 km^3. For the warm Mars scenario (not shown), habitable volumes for mesophiles (20–50 °C) generally decreased, and those for thermophiles (50–80 °C) and hyperthermophiles (80–110 °C) generally increased, particularly during the early stages of variable-flux bombardments. Despite intrinsic differences between the two worlds (mass, heliocentric distance), we find that this observed trend for the habitability of Noachian Mars' crust as tied to the early bombardment regime closely mimics that described in Abramov and Mojzsis (2009) for Hadean Earth.

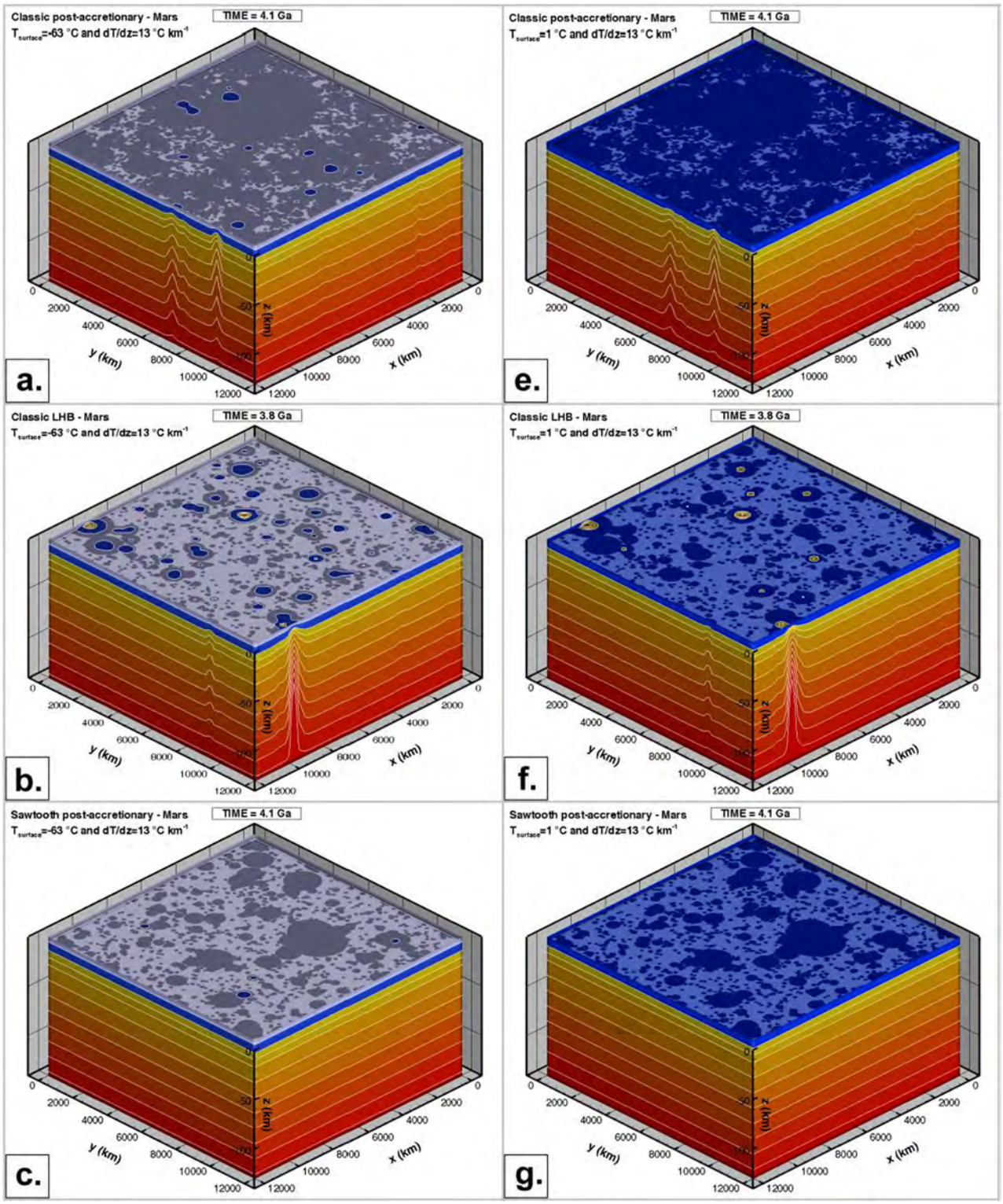

Fig. 5. (*Continued on the next page*) A three-dimensional thermal model representing the upper 140 km of Mars at the end of the bombardment. Only impactors larger than 2.5 km in diameter are included. Dark circles indicate crater locations, light blue areas indicate the extent of the cryosphere, and dark blue areas indicate the extent of the subsurface habitable zone. The upper boundary shows temperatures at a depth of 4 km. (a–d) Classical post-accretionary (cPA), classical LHB (cLHB), Sawtooth post-accretionary (sPA), and Sawtooth LHB scenarios (sLHB), respectively, with a surface temperature of $-63\,^{\circ}\mathrm{C\,km^{-1}}$. (e–h) Classical post-accretionary (cPA), classical LHB (cLHB), Sawtooth post-accretionary (sPA), and Sawtooth LHB scenarios (sLHB), respectively, with a surface temperature of $1\,^{\circ}\mathrm{C\,km^{-1}}$. (For interpretation of the references to color in this figure legend, the reader is referred to the web version of this article.)

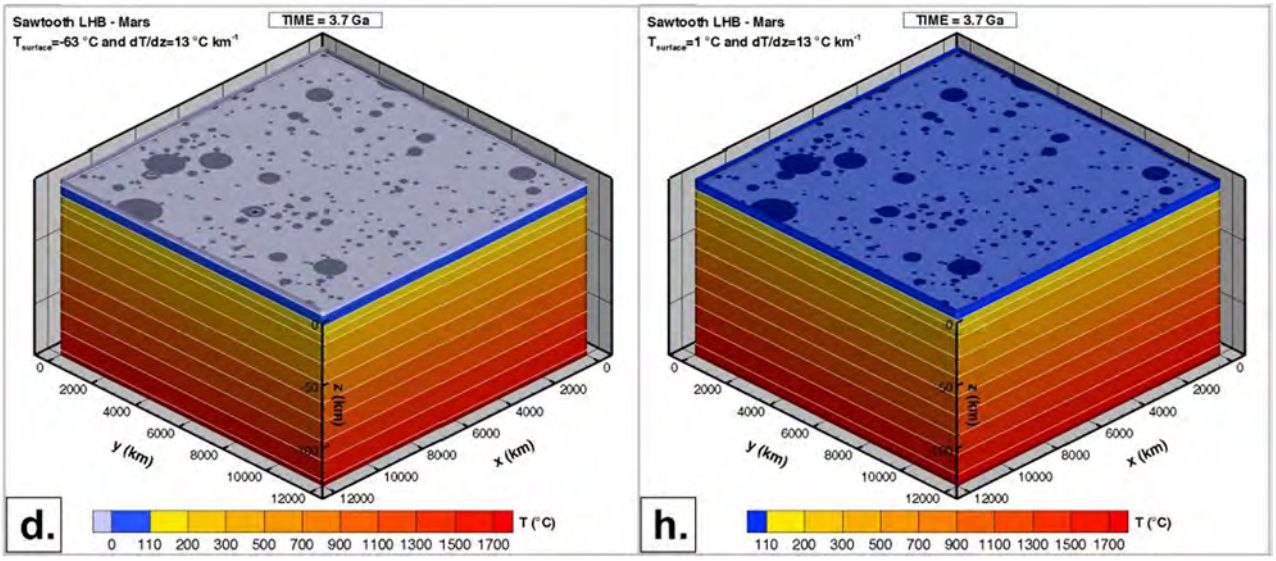

Fig. 5. (*continued*)

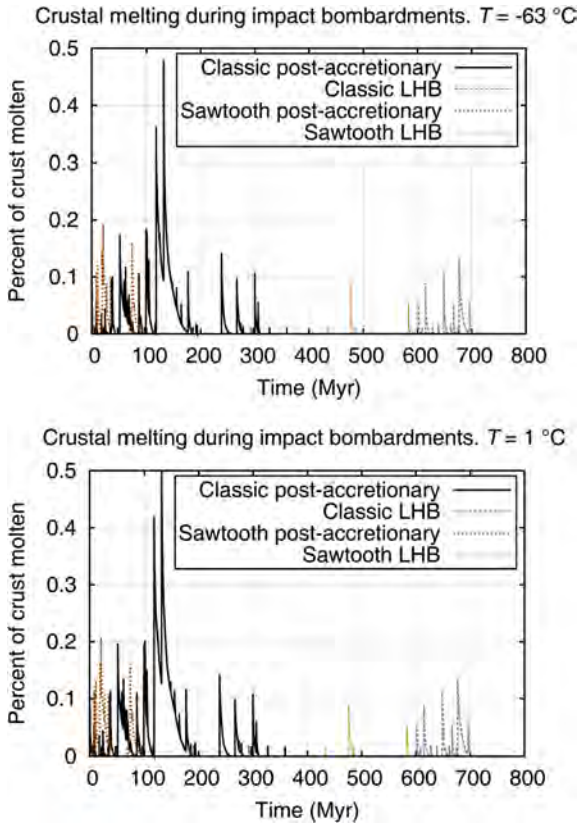

Fig. 6. The amount of melting in the upper 20 km of the martian crust during impact bombardments. Derived from the three-dimensional transient thermal model. Melt deposited in ejecta blankets is not included. (Top) The effects of classical post-accretionary (cPA), classical LHB (cLHB), Sawtooth post-accretionary (sPA), and Sawtooth LHB (sLHB) scenarios with a surface temperature of $-63\,^{\circ}\mathrm{C\,km^{-1}}$. (Bottom) The effects of classical post-accretionary (cPA), classical LHB (cLHB), Sawtooth post-accretionary (sPA), and Sawtooth LHB (sLHB) scenarios with a surface temperature of $1\,^{\circ}\mathrm{C\,km^{-1}}$.

The geophysical habitable volumes in active impact-induced hydrothermal systems were also gaged, and are shown in Fig. 8 for the warm Mars scenario. It is important to note that for the cold early Mars simulations, essentially all water ice melting within the cryosphere could be considered hydrothermal, and Fig. 7 provides a good approximation for these hydrothermal volumes. For our purposes, "hydrothermal volume" is defined as a volume within the upper 4 km of the crust that has been elevated to a temperature at least twice that produced by a normal geothermal gradient. As with the habitable volumes in Fig. 7, hydrothermal habitable volumes increased during the early stages of impact bombardments and decreased during the later stages, with the exception of the constant-flux cLHB, in which they achieved a steady-state after the initial increase. It is evident from these results that water ice (and associated D/H signatures) in the cryosphere on Mars must post-date, possibly significantly, the bombardment epoch (cf. Usui et al., 2015).

5. Discussion

The results of this study are necessarily sensitive to the parameters of a particular bombardment scenario, in particular total delivered mass, size-frequency distribution, impact velocities, and time dependence of the impacts. Assuming a constant impact velocity, the total energy of the bombardment scales linearly with total delivered mass and with the square of the impact velocity. The size-frequency distribution of the impactor population determines, among other things, the mean depth at which impact-delivered energy is deposited in planetary interiors.

Time-dependence of the impacts has a relatively small effect on crustal melting as only a small percentage of the crust is molten due to impacts at any given time (Fig. 6), but has a more significant effect on habitability due to lower temperatures and thus higher volumes (Fig. 7). It is noteworthy that, although the specifics of the bombardments investigated in this study will likely continue to be revised (cf. Kaib and Chambers, 2016) these scenarios bracket the general possibilities for early planetary bombardments, and it is possible to approximately interpolate and/or extrapolate the results of this study using the general relationships described above.

Impact events on Noachian Mars were rarely harmful for any hypothetical biome (obviously based on the singular example from Earth) that may have existed in the crust at that time. Low impact velocities mean that relatively little crustal melting took place even following very large impacts. We find that a classical LHB on Noachian Mars yields total impact-generated thermophilic and hydrothermal habitable volumes smaller by a factor of $\sim$5 compared to the Hadean Earth values reported in Abramov and Mojzsis (2009). This is primarily due to the combination of reduced sur-

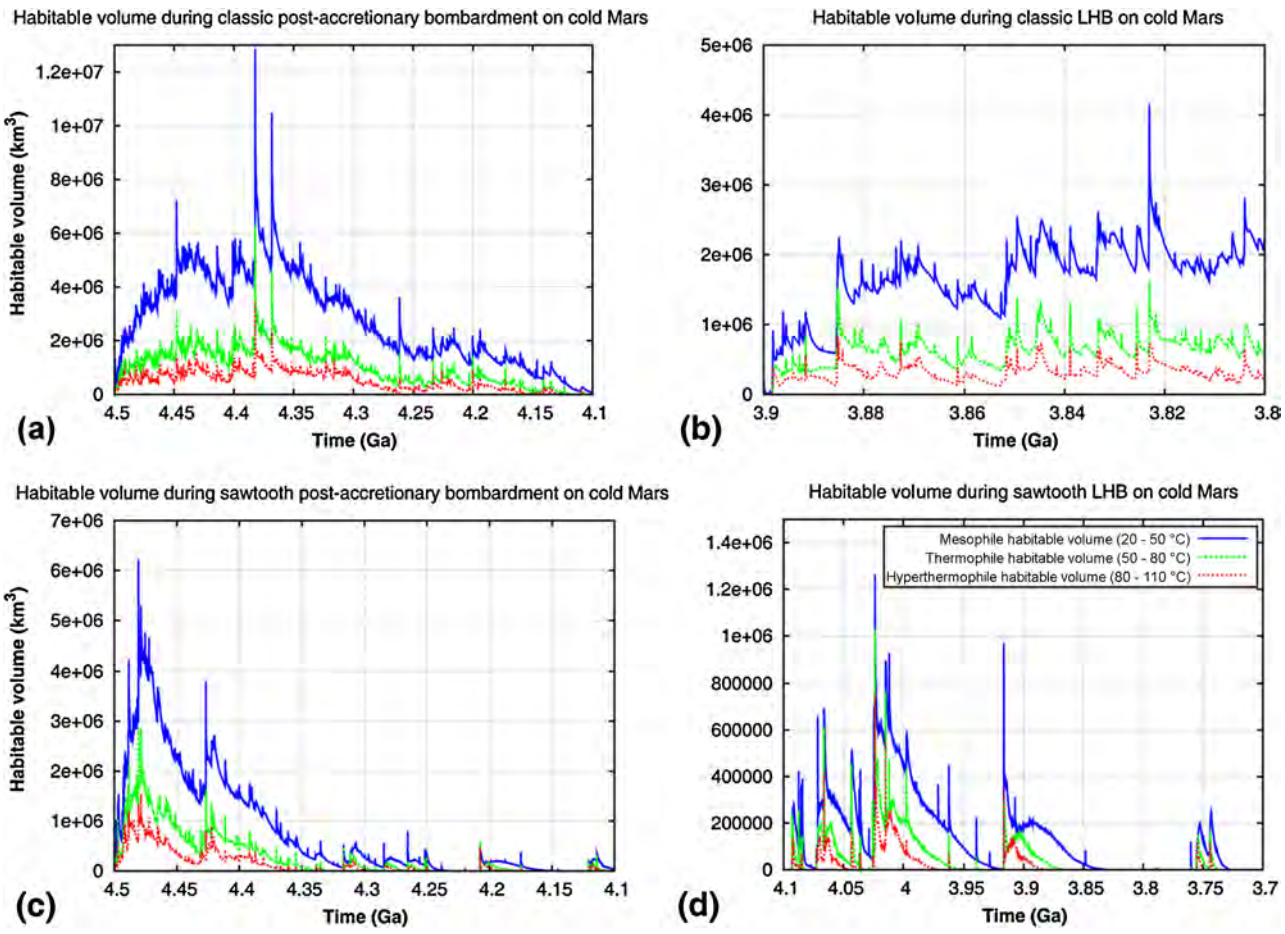

Fig. 7. Global habitable volumes for mesophiles (20–50 °C, blue), thermophiles (50–80 °C, green) and hyperthermophiles (80–110 °C, red) in the upper of 4 km of the crust during impact bombardments on cold early Mars. Surface temperature is −63 °C. Derived from the three-dimensional transient thermal model. Only impactors larger than 2.5 km are included. (a) Habitable volumes during the classical post-accretionary (cPA) scenario. (b) Habitable volumes during the classical LHB (cLHB) scenario. (c) Habitable volumes during the Sawtooth post-accretionary (sPA) scenario. (d) Habitable volumes during the Sawtooth LHB (sLHB). (For interpretation of the references to color in this figure legend, the reader is referred to the web version of this article.)

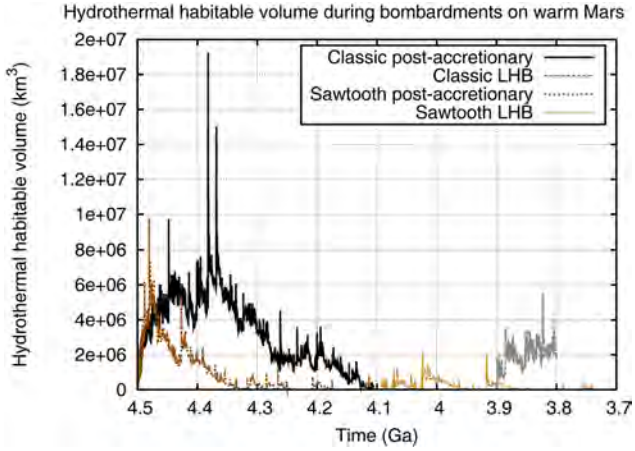

Fig. 8. Global habitable volumes for thermophiles (50–80 °C) and hyperthermophiles (80–110 °C) in active hydrothermal environments in the upper of 4 km of the crust during impact bombardments on warm early Mars. Surface temperature is 1 °C. Derived from the three-dimensional transient thermal model. Only impactors larger than 2.5 km are included.

face area and lower impact velocities. When considered as number of impacts per surface area, however, the potential benefit to a postulated biome from abundant hydrothermal system generation arising from a higher flux of impactors may have been more important on Mars compared to Earth. The above calculations assume a geothermal heat flux roughly equivalent to that of the Hadean Earth (e.g., Korenaga, 2006); uncertainties over which values to use also means that this could have been a factor of ∼5 higher (e.g., Abramov et al., 2013). Thus, depending on the geotherm adopted in these models, this difference would have reduced the extent of the subsurface habitable zone on Earth, making total impact-generated thermophilic and hydrothermal habitable volumes comparable between the two planets.

Although evidence has mounted that the Hadean Earth possessed a thick atmosphere and stable liquid water on its surface for at least the last 4 Gyr (e.g., Mojzsis and Harrison, 2000; Mojzsis et al., 2001), considerable debate reigns over whether Mars was *ever* warm and wet, even in its early days (Wordsworth et al., 2015). If the average martian surface temperature at the LHB was comparable to contemporary values (−63 °C), life may have persisted in a global liquid water aquifer deep beneath the cryosphere (Clifford, 1993). Over 10^5–10^6 of the impact craters that formed during the LHB and post-accretionary bombardment, respectively, would have accessed this postulated global aquifer by puncturing the cryosphere layer, thus providing a subsurface plumbing network between individual impact-induced hydrothermal systems (Schwenzer et al., 2012).

Reduced gravity on Mars, compared to the Earth, introduces another factor that favors the maintenance of a deep martian microbial biome: larger subsurface pore spaces. The porosity of loose material such as regolith generally decreases exponentially with depth with the closure of pore spaces as a function of lithostatic

pressure (e.g., Binder and Lange, 1980). The same mechanism leads to internal collapse (healing) of rock fractures and other living space deeper in the crust. Due to Mars' substantially lower gravity (0.376 that of Earth), pore spaces at a depth of 4 km are expected to be about an order of magnitude larger than those on Earth. Impact-induced subsurface fracturing (e.g., Nordyke, 1964) would have been greater on early Mars compared to early Earth due to the higher impact flux per unit area.

Thermal effects of impact bombardments on Mars associated with smaller craters were important, but only at the local scale. For example, the heat generated within a ~60-km impact crater has the capacity to denature pre-existing phyllosilicates (Fairen et al., 2010), making them undetectable by spectroscopy. An impact of that magnitude also would have initiated a hydrothermal system lasting over 10^5 yr, provided that water was present in the subsurface (Abramov and Kring, 2005). Hydrothermal fields provide energetically-rich habitats for a vast variety of microorganisms. It also would have released significant amounts of water vapor into the atmosphere, as a result of both the impact itself and post-impact hydrothermal activity, temporarily warming the climate (e.g., Segura et al., 2002).

6. Conclusions

From the mass and size-frequency distribution constraints, the largest impactor in our baseline Noachian Mars LHB model is ~250 km in diameter. This would have generated a crater ~1800 km in diameter, or approximately the same size as Argyre Basin. The largest impactor in the martian baseline post-accretionary model (cPA) is ~490 km in diameter. The classical post-accretionary scenario (cPA) has the largest amount of mass delivered, followed by the Sawtooth post-accretionary (sPA), classical LHB (cLHB), and Sawtooth LHB (sLHB) scenarios.

As was the case for model studies of Hadean–Eoarchean Earth bombardment (Abramov and Mojzsis, 2009; Abramov et al., 2013), we find that most of the martian crust escaped *melting* by either a post-accretionary or a late bombardment even if it was *mechanically* destroyed. In our evaluation of classical post-accretion (cPA) scenario to Noachian Mars, which has the highest delivered mass of our models, we find that a maximum of ~0.5% of the upper crust is molten at any given time. The total cumulative melt production on Mars in the bombardment epoch, as a percentage of total crustal volume, was 3.9% in the classical post-accretionary scenario, 1.1% in the Sawtooth post-accretionary scenario, 0.8% in the classical LHB scenario, and 0.2% in the Sawtooth LHB scenario. The surface effects of bombardments from mechanical and chemical modifications were far more pronounced than those induced by melting. The models reveal resurfacing percentages of 100%, 46%, 36%, and 10% for the classical post-accretionary, Sawtooth post-accretionary, classical LHB, and Sawtooth LHB, respectively.

On Mars, impacts giveth more than impacts taketh away (after McKinnon, 1989). Our analysis shows that impact bombardments greatly enhanced the geophysical habitable zone of Noachian Mars by creating new habitable hydrothermal environments with abundant free-energy from chemical disequilibria; just as this was happening on Earth with the emergence of the terrestrial biosphere before ca. 3830 Ma (Mojzsis et al., 1996), or perhaps earlier (ca. 4100 Ma; Bell et al., 2015). We also find that the consequences of early impact processes are particularly acute in models that simulate a "cold early Mars", in which the near-subsurface is frozen to a depth of several kilometers. Under such prevailing cold and arid conditions, impact-generated habitable volumes reached maxima of $\sim 1.2 \times 10^7$ and $\sim 4 \times 10^6$ km^3 ($\leq$0.5% of Mars' total crustal volume) for classical post-accretionary bombardment and classical LHB, respectively.

Acknowledgements

This work benefited from discussions and debates with W.F. Bottke, R. Brasser, Á. Keresztúri, D.A. Kring and S. Marchi. OA acknowledges the NASA Mars Fundamental Research Program (NNH14AX55I) in support of this work. SJM is grateful for support from the John Templeton Foundation – FfAME Origins program, the NASA Exobiology Program under grant NNH14ZDA001N-EXO, and the NASA Cosmochemistry Program (NNH13ZDA001N-COS). SJM also acknowledges sabbatical leave support from the Earth-Life Science Institute (ELSI) at Tokyo Institute of Technology. Copyediting by USGS volunteer K. Bebell is also gratefully acknowledged. A portion of the manuscript was completed while SJM was in residence as a Distinguished Research Professor at the Institute for Geological and Geochemical Research, Research Center for Astronomy and Earth Sciences of the Hungarian Academy of Sciences. This is a contribution of the Collaborative for Research in Origins (CRiO), which is funded by the John Templeton Foundation.

Appendix A. Supplementary material

Supplementary material related to this article can be found online at http://dx.doi.org/10.1016/j.epsl.2016.02.035.

References

Abbott, S.S., Harrison, T.M., Schmitt, A.K., Mojzsis, S.J., 2012. A search for thermal excursions from ancient extraterrestrial impacts using Hadean zircon Ti–U–Th–Pb depth profiles. Proc. Natl. Acad. Sci. 109, 13486–13492.

Abramov, O., Kring, D.A., 2005. Impact-induced hydrothermal activity on Early Mars. J. Geophys. Res. 110, E12S09. http://dx.doi.org/10.1029/2005JE002453.

Abramov, O., Mojzsis, S.J., 2009. Microbial habitability of the Hadean Earth during the late heavy bombardment. Nature 459, 419–422.

Abramov, O., Kring, D.A., Mojzsis, S.J., 2013. The impact environment of the Hadean Earth. Chem. Erde, Geochem. 73 (3), 227–248. http://dx.doi.org/10.1016/j.chemer.2013.08.004.

Andrews-Hanna, J.C., Zuber, M.T., Banerdt, W.B., 2008. The Borealis basin and the origin of the martian crustal dichotomy. Nature 453 (7199), 1212–1215.

Ash, R.D., Knott, S.F., Turner, G., 1996. A 4-Gyr shock age for a Martian meteorite and implications for the cratering history of Mars. Nature 380, 57–59.

Babeyko, A.Yu., Zharkov, V.N., 2000. Martian crust: a modeling approach. Phys. Earth Planet. Inter. 117, 421–435.

Bell, E.A., Harrison, T.M., Kohl, I.E., Young, E.D., 2014. Eoarchean crustal evolution of the Jack Hills zircon source and loss of Hadean crust. Geochim. Cosmochim. Acta 146, 27–42.

Bell, E.A., Boehnke, P., Harrison, T.M., Mao, W.L., 2015. Potentially biogenic carbon preserved in a 4.1 billion-year-old zircon. Proc. Natl. Acad. Sci. 112.

Binder, A.B., Lange, M.A., 1980. On the thermal history, thermal state, and related tectonism of a moon of fission origin. J. Geophys. Res. 85, 3194–3208.

Bottke, W.F., Durda, D.D., Nesvorny, D., Jedicke, R., Morbidelli, A., Vokrouhlicky, D., Levison, H., 2005. The fossilized size distribution of the main asteroid belt. Icarus 175, 111–140.

Bottke, W.F., Walker, R.J., Day, J.M.D., Nesvorný, D., Elkins-Tanton, L., 2010. Stochastic Late Accretion to Earth, the Moon, and Mars. Science 330, 1527–1530.

Bottke, W.F., Vokrouhlický, D., Minton, D.A., Nesvorný, D., Morbidelli, A., Brasser, R., Simonson, B., Levison, H.F., 2012. An Archaean heavy bombardment produced by a destabilized extension of the asteroid belt. Nature 485, 78–81.

Carr, M.H., 1999. Retention of an atmosphere on early Mars. J. Geophys. Res. 104, 21897–21909. http://dx.doi.org/10.1029/1999JE001048.

Carr, M.H., 2012. The fluvial history of Mars. Philos. Trans. R. Soc. A, Math. Phys. Eng. Sci. 370 (1966), 2193–2215.

Carr, M.H., Head, J.W., 2010. Geologic history of Mars. Earth Planet. Sci. Lett. 294 (3), 185–203.

Childs, K.W., 1993. HEATING 7.2 User's Manual, ORNL/TM-12262. Oak Ridge National Laboratory.

Clifford, S.M., 1993. A model for the hydrologic and climate behaviour of water on Mars. J. Geophys. Res. 98, 10973–11016.

Craddock, R.A., Howard, A.D., 2002. The case for rainfall on a warm, wet early Mars. J. Geophys. Res., Planets 107 (E11), 21-1.

Dauphas, N., Pourmand, A., 2011. Hf–W–Th evidence for rapid growth of Mars and its status as a planetary embryo. Nature 473 (7348), 489–492.

De Niem, D., Kührt, E., Morbidelli, A., Motschmann, U., 2012. Atmospheric erosion and replenishment induced by impacts upon the Earth and Mars during a heavy bombardment. Icarus 221 (2), 495–507. http://dx.doi.org/10.1016/j.icarus.2012.07.032.

Dohm, J.M., Hare, T.M., Robbins, S.J., Williams, J.P., Soare, R.J., El-Maarry, M.R., Maruyama, S., 2015. Geological and hydrological histories of the Argyre province, Mars. Icarus 253, 66–98.
Ehlmann, B.L., Mustard, J.F., Bishop, J.L., Swayze, G.A., Clark, R.N., Bishop, J.L., Poulet, F., Des Marais, D.J., Roach, L.H., Milliken, R.E., Wray, J.J., Barnouin-Jha, O., Murchie, S.L., 2009. Identification of hydrated silicate minerals on Mars using MRO-CRISM: geologic context near Nili Fossae and implications for aqueous alteration. J. Geophys. Res. 114. http://dx.doi.org/10.1029/2009JE003339.
Fairen, A.G., Chevrier, V., Abramov, O., Marzo, G.A., Gavin, P., Davila, A.F., McKay, C.P., 2010. Noachian and more recent phyllosilicates in impact craters on Mars. Proc. Natl. Acad. Sci. 107 (27), 12095–12100. http://dx.doi.org/10.1073/pnas.1002889107.
Fairén, A.G., 2010. A cold and wet Mars. Icarus 208 (1), 165–175.
Flynn, G.J., 1996. The delivery of organic matter from asteroids and comets to the early surface of Mars. Earth Moon Planets 72 (1–3), 469–474.
Frey, H., 2008. Ages of very large impact basins on Mars: implications for the late heavy bombardment in the inner Solar System. Geophys. Res. Lett. 35, L13203. http://dx.doi.org/10.1029/2008GL033515.
Gault, D.E., Heitowit, E.D., 1963. The partition of energy for hypervelocity impact craters formed in rock. In: Proc. 6th Hypervelocity Impact Symp., vol. 2 (2), pp. 419–456. April.
Gomes, R., Levison, H.F., Tsiganis, K., Morbidelli, A., 2005. Origin of the cataclysmic Late Heavy Bombardment period of the terrestrial planets. Nature 435, 466–469.
Hart, M.H., 1979. Habitable zones about main sequence stars. Icarus 37 (1), 351–357.
Hartmann, W.K., 1966. Early lunar cratering. Icarus 5, 406–418.
Hopkins, M.D., Mojzsis, S.J., 2015. A protracted timeline for lunar bombardment from mineral chemistry, Ti thermometry and U–Pb geochronology of Apollo 14 melt breccia zircons. Contrib. Mineral. Petrol. 169 (3), 1–18.
Horner, J., Mousis, O., Petit, J.-M., Jones, B.W., 2009. Differences between the impact regimes of the terrestrial planets: implications for primordial D:H ratios. Planet. Space Sci. 57 (12), 1338–1345. http://dx.doi.org/10.1016/j.pss.2009.06.006.
Ivanov, B.A., 2001. Mars/Moon cratering ratio estimates. Space Sci. Rev. 60, 87–104.
Ivanov, B.A., Neukum, G., Bottke, W.F., Hartmann, W.K., 2002. The comparison of size-frequency distributions of impact craters and asteroids and the planetary cratering rate. In: Bottke, W.F., Cellino, A., Paolicchi, P., Binzel, R.P. (Eds.), Asteroids III. University of Arizona Press, pp. 89–101.
JeongAhn, Y., Malhotra, R., 2015. The current impact flux on Mars and its seasonal variation. arXiv:1503.03885.
Kaib, N.A., Chambers, J.E., 2016. The fragility of the terrestrial planets during a giant-planet instability. Mon. Not. R. Astron. Soc. 455 (4), 3561–3569. http://dx.doi.org/10.1093/mnras/stv2554.
Kieffer, S.W., Simonds, C.H., 1980. The role of volatiles and lithology on the impact cratering process. Rev. Geophys. 18, 143–181.
Korenaga, J., 2006. Archean geodynamics and the thermal evolution of Earth. In: Benn, K., Mareschal, J.-C., Condie, K.C. (Eds.), Archean Geodynamics and Environments. Washington, DC. In: AGU Geophys. Monogr., vol. 164, pp. 7–32.
Kring, D.A., Cohen, B.A., 2002. Cataclysmic bombardment throughout the inner solar system 3.9–4.0 Ga. J. Geophys. Res. 107 (E2), 5009. http://dx.doi.org/10.1029/2001JE001529.
Le Feuvre, M., Wieczorek, M.A., 2011. Nonuniform cratering of the Moon and a revised crater chronology of the inner Solar System. Icarus 214 (1), 1–20. http://dx.doi.org/10.1016/j.icarus.2011.03.010.
Levison, H.F., Dones, L., Duncan, M.J., 2001. The origin of Halley-type comets: probing the inner Oort cloud. Astron. J. 121, 2253–2267.
Marchi, S., Bottke, W.F., Morbidelli, A., Kring, D., 2012. The onset of the lunar cataclysm as recorded in its ancient crater populations. Earth Planet. Sci. Lett. 325–326, 27–38.
Marchi, S., Bottke, W.F., Cohen, B.A., Wuennemann, K., Kring, D.A., McSween, H.Y., De Sanctis, M.C., O'Brien, D.P., Schenk, P., Raymond, C.A., Russell, C.T., 2013. High velocity collisions from the lunar cataclysm recorded in asteroidal meteorites. Nat. Geosci. 6, 303–307.
Marchi, S., Bottke, W.F., Elkins-Tanton, L.T., Bierhaus, M., Wuennemann, K., Morbidelli, A., Kring, D.A., 2014. Widespread mixing and burial of Earth's Hadean crust by asteroid impacts. Nature 511, 578–582.
Maurer, P., Eberhardt, P., Geiss, J., Grögler, N., Stettler, A., Brown, G.M., Krähenbühl, U., 1978. Pre-Imbrian craters and basins: ages, compositions and excavation depths of Apollo 16 breccias. Geochim. Cosmochim. Acta 42 (11), 1687–1720.
McKinnon, W.B., 1989. Impacts giveth and impacts taketh away. Nature 338 (6215), 465–466.
McSween, H.Y., Grove, T.L., Wyatt, M.B., 2003. Constraints on the composition and petrogenesis of the martian crust. J. Geophys. Res. 108 (E12), 5135. http://dx.doi.org/10.1029/2003JE002175.
Melosh, H.J., 1989. Impact Cratering: a Geologic Process. Oxford Univ. Press, New York.
Melosh, H.J., 2008. Did an impact blast away half of the martian crust? Nat. Geosci. 1 (7), 412–414.
Minton, D.A., Malhotra, R., 2009. A record of planet migration in the main asteroid belt. Nature 457, 1109–1111.
Mojzsis, S.J., Harrison, T.M., 2000. Vestiges of a beginning: clues to the emergent biosphere recorded in the oldest known sedimentary rocks. GSA Today 10 (4), 1–6.
Mojzsis, S.J., Arrhenius, G., McKeegan, K.D., Harrison, T.M., Nutman, A.P., Friend, C.R., 1996. Evidence for life on Earth before 3800 million years ago. Nature 384, 55–59.
Mojzsis, S.J., Harrison, T.M., Pidgeon, R.T., 2001. Oxygen-isotope evidence from ancient zircons for liquid water at the Earth's surface 4300 Myr ago. Nature 409 (6817), 178–181.
Morbidelli, A., Marchi, S., Bottke, W.F., Kring, D.A., 2012. A sawtooth-like timeline for the first billion years of lunar bombardment. Earth Planet. Sci. Lett. 355–356, 144–151.
Neukum, G., 1983. Meteoritenbombardement und Datierung planetarer Oberflächen. Habilitation Dissertation for Faculty Membership. University of Munich, 186 pp.
Neukum, G., Ivanov, B.A., 1994. Crater size distributions and impact probabilities on Earth from lunar, terrestrial-planet, and asteroid cratering data. In: Gehrels, T., Matthews, M.S., Schumann, A. (Eds.), Hazards Due to Comets and Asteroids. University of Arizona Press, Tucson, AZ, 359 p.
Neukum, G., Ivanov, B., Hartmann, W.K., 2001. Cratering records in the inner solar system. In: Kallenbach, R., et al. (Eds.), Chronology and Evolution of Mars. Kluwer, Dordrecht, pp. 55–86.
Neumann, G.A., Zuber, M.T., Wieczorek, M.A., McGovern, P.J., Lemoine, F.G., Smith, D.E., 2004. Crustal structure of Mars from gravity and topography. J. Geophys. Res., Planets 109 (E8).
Nordyke, M.D., 1964. Cratering experience with chemical and nuclear explosives. In: Proceedings of the Third Plowshare Symposium—Engineering with Nuclear Explosives, U.S. At. Energy Comm. Rep. TID-7695. Washington, DC, pp. 51–73.
Nutman, A.P., Friend, C.R., Bennett, V.C., 2001. Review of the oldest (4400–3600 Ma) geological and mineralogical record: glimpses of the beginning. Episodes 24 (2), 93–101.
Öpik, E.J., 1960. The lunar surface as an impact counter. Mon. Not. R. Astron. Soc. 120, 404–411.
Pierazzo, E., Collins, G., 2004. A brief introduction to hydrocode modeling of impact cratering. In: Cratering in Marine Environments and on Ice. Springer, Berlin, Heidelberg, pp. 323–340.
Pierazzo, E., Artemieva, N.A., Ivanov, B.A., 2005. Starting conditions for hydrothermal systems underneath Martian craters: hydrocode modeling. In: Kenkmann, T., Hörz, F., Deutsch, A. (Eds.), Large Meteorite Impacts III. In: Spec. Pap., Geol. Soc. Am., vol. 384. Springer, pp. 443–457.
Richardson, J.E., Melosh, H.J., Greenberg, R.J., O'Brien, D.P., 2005. The global effects of impact-induced seismic activity on fractured asteroid surface morphology. Icarus 179, 325–349.
Ryder, G., 1990. Lunar samples, lunar accretion and the early bombardment of the Moon. Eos 71, 313–323.
Ryder, G., 2002. Mass flux in the ancient Earth–Moon system and benign implications for the origin of life on Earth. J. Geophys. Res. 107, 6. http://dx.doi.org/10.1029/2001JE001583.
Ryder, G., Koeberl, C., Mojzsis, S.J., 2000. Heavy Bombardment of the Earth at −3.85 Ga: the search for petrographic and geochemical evidence. In: Canup, R., Righter, K. (Eds.), Origin of the Earth and Moon. University of Arizona Press, Tucson, pp. 475–492.
Sautter, V., Toplis, M.J., Wiens, R.C., Cousin, A., Fabre, C., Gasnault, O., Wray, J.J., 2015. In situ evidence for continental crust on early Mars. Nat. Geosci. 8, 605–609.
Schaeffer, O.A., Husain, L., 1974. Chronology of lunar basin formation. In: Lunar and Planetary Science Conference Proceedings, vol. 5, pp. 1541–1555.
Schmidt, R.M., Housen, K.R., 1987. Some recent advances in the scaling of impact and explosion cratering. Int. J. Impact Eng. 5, 543–560.
Schwenzer, S.P., Abramov, O., Allen, C.C., Clifford, S.M., Cockell, C.S., Filiberto, J., Kring, D.A., Lasue, J., McGovern, P.J., Newsom, H.E., Treiman, A.H., Vaniman, D.T., Wiens, R.C., 2012. Puncturing Mars: how impact craters interact with the Martian cryosphere. Earth Planet. Sci. Lett. 335, 9–17.
Segura, T.L., Toon, O.B., Colaprete, A., Zahnle, K., 2002. Environmental effects of large impacts on Mars. Science 298, 1977–1980.
Shoemaker, E.M., 1962. Interpretation of lunar craters. In: Kopal, Z. (Ed.), Physics and Astronomy of the Moon. Academic Press, San Diego, pp. 283–359.
Sleep, N.H., Zahnle, K., 1998. Refugia from asteroid impacts on early Mars and the early Earth. J. Geophys. Res. 103, 28529–28544.
Strom, R.G., Malhotra, R., Ito, T., Yoshida, F., Kring, D.A., 2005. The origin of planetary impactors in the inner solar system. Science 309, 1847–1850.
Swindle, T.D., Isachsen, C.E., Weirich, J.R., Kring, D.A., 2009. ^{40}Ar–^{39}Ar ages of H chondrite impact melt breccias. Meteorit. Planet. Sci. 44, 747–762.
Tanaka, K.L., 1986. The stratigraphy of Mars. In: Seventeenth Lunar and Planetary Science Conference Part 1. J. Geophys. Res. 91 (B13), E139–E158.
Taylor, S.R., McLennan, S.M., 1995. The geochemical evolution of the continental crust. Rev. Geophys. 33 (2), 241–265.
Tera, F., Papanastassiou, D.A., Wasserburg, G.J., 1974. Isotopic evidence for a terminal lunar cataclysm. Earth Planet. Sci. Lett. 22, 1–21.
Toon, O.B., Pollack, J.B., Ackerman, T.P., Turco, R.P., McKay, C.P., Liu, M.S., 1982. Evolution of an impact-generated dust cloud and its effects on the atmosphere. Spec. Pap., Geol. Soc. Am. 190, 187–200.
Trail, D., Mojzsis, S.J., Harrison, T.M., 2007. Thermal events documented in Hadean zircons by ion microprobe depth profiles. Geochim. Cosmochim. Acta 71, 4044–4065.

Tsiganis, K., Gomes, R., Morbidelli, A., Levison, H.F., 2005. Origin of the orbital architecture of the giant planets of the Solar System. Nature 435 (7041), 459–461.

Turner, G., Cadogan, P.H., Yonge, C.J., 1973. Argon selenochronology. In: Proceedings of the Fourth Lunar Science Conference. Geochim. Cosmochim. Acta 2 (Supplement 4), 1889–1914.

Turner, G., 1979. A Monte Carlo fragmentation model for the production of meteorites: implications for gas retention ages. Proc. Lunar Planet. Sci. Conf. X, 1917–1941.

Usui, T., Alexander, C.M.O'D., Wang, J., Simon, J.I., Jones, J.H., 2015. Meteoritic evidence for a previously unrecognized hydrogen reservoir on Mars. Earth Planet. Sci. Lett. 410, 140–151.

Walker, R.J., 2009. Highly siderophile elements in the Earth, Moon and Mars: update and implications for planetary accretion and differentiation. Chem. Erde, Geochem. 69, 101–125.

Werner, S.C., 2014. Moon, Mars, Mercury: basin formation ages and implications for the maximum surface age and the migration of gaseous planets. Earth Planet. Sci. Lett. 400, 54–65.

Wetherill, B., 1975. Late heavy bombardment of the Moon and terrestrial planets. Proc. Lunar Planet. Sci. Conf. VIII, 1–16.

Wieczorek, M.A., Zuber, M.T., 2004. Thickness of the Martian crust: improved constraints from geoid-to-topography ratios. J. Geophys. Res., Planets 109 (E1).

Wordsworth, R.D., Kerber, L., Pierrehumbert, R.T., Forget, F., Head, J.W., 2015. Comparison of "warm and wet" and "cold and icy" scenarios for early Mars in a 3-D climate model. J. Geophys. Res., Planets 120 (6), 1201–1219.

Wright, I.P., Grady, M.M., Pillinger, C.T., 1989. Organic materials in a Martian meteorite. Nature 340, 220–222.

Oleg Abramov is a Research Space Scientist at the United States Geological Survey's Astrogeology Science Center in Flagstaff, Arizona. His research includes serving as Co-Investigator on the *Europa-THEMIS* instrument, exploring the thermal effects of impact bombardments on terrestrial planets, usage of Unmanned Aerial Systems, numerical modeling of hydrothermal activity on present-day Mars, and *Cassini* data analysis. He also serves as Project Manager for image processing support for the *OSIRIS REx* mission.

Steve Mojzsis is Professor of Geology at the Department of Geological Sciences, University of Colorado at Boulder where he directs the Collaborative for Research in Origins (*CRiO*) funded by the John Templeton Foundation – FfAME Origins program. He is also a Distinguished Visiting Professor at the Hungarian Academy of Sciences in Budapest, and has held visiting academic positions in France at the Université Claude Bernard Lyon 1, and the Centre de Recherches Pétrographiques et Géochimiques (CRPG) in Nancy, and in Japan at the Earth-Life Science Institute (ELSI) at the Tokyo Institute of Technology. His research seeks to understand the physical and chemical conditions on planets that lead to emergence of a biosphere.